Integrating Tensile Parameters in 3D Mass-Spring System

V. Baudet[1] and M. Beuve[2] and F. Jaillet[2] and B. Shariat[2] and F. Zara [2]

[1]LSIIT-IGG, UMR CNRS 7005, Illkirch, F-67412, France
[2]LIRIS-SAARA, UMR CNRS 5205, Univiversity of Lyon 1, Villeurbanne, F-69622, France

Abstract

Besides finite element method, mass-spring discrete modeling is widely used in computer graphics. This discrete model allows to perform very easily interactive deformations and to handle quite complex interactions with only a few equations. Thus, it is perfectly adapted to generate visually correct animations. However, a drawback of this simple formulation is the relative difficulty to control efficiently physically realistic behaviors. Indeed, none of the existing models has succeeded in dealing with this satisfyingly. Here, we propose a new general 3D formulation that reconstructs the geometrical model as an assembly of elementary "bricks". Each brick (or element) is then transformed into a mass-spring system. Edges are replaced by springs that connect masses representing the element vertices. The key point of our approach is the determination of the spring-stiffness to reproduce the correct mechanical properties (Young's modulus, Poisson's ratio, bulk and shear modulus) of the reconstructed object. We validate our methodology by performing some numerical experimentations, like shearing and loading, or beam deflection and then we evaluate the accuracy limits of our approach.

1. Introduction

Models based on the resolution of continuous-media-mechanics equations by finite elements methods are generally applied to accurately simulate the deformations of 3D objects. However, they require a rigorous description of the boundary conditions, which is hardly compatible with any unpredictable interactions. Moreover, the amplitudes of the applied strains and stresses must be well defined in advance to choose either a small - with Cauchy's description - or a large deformation context - with St Venant Kirchoff's description. Indeed, the accuracy of each context is optimized to its domain of deformation.

In the literature, discrete models (like mass-spring systems) widely used in computer-graphics animation are generally proposed to deal with interactive applications and to allow unpredictable interactions. They are adapted to virtual reality environments where many unpredicted collisions may occur and objects can undergo large or small deformations. Medical or surgery simulators present another example of their possible applications. Nevertheless these models generally fail to represent accurately the behavior of real objects.

In this paper, we propose a new method that gathers the advantages of both approaches. Section 2 presents some previous work on mass-spring systems and particularly their parameterization and section 3 presents a survey of some mechanical parameters. Then in section 4, we propose our 3D mass-spring model in which stiffness constants are calculated according to tensile parameters of the simulated object. Section 5 presents an evaluation of our model through numerical experiments. Finally some concluding remarks and perspectives are given in section 6.

2. Related Work

Mass-spring systems have largely been used in the animation context, because of their simple implementation and their possible applications for a large panel of deformations. They consist in describing a surface or a volume with a mesh in which the global mass is uniformly distributed over the mesh nodes. The tensile behavior of the object is simulated by the action of springs, linking the mesh nodes. Then, Newton's laws govern the dynamics of the model.

Mass-spring systems have been used to model textiles [KEH04, LJF*91, Pro95], long animals such as

snakes [Mil88], or soft organic tissues, such as muscles, face or abdomen, with sometimes the possibility to simulate tissue cut [AT00, CHP89, MLM*05, MC97, NT98, Pal03, PBP96]. Moreover, these systems have been used to describe a wide range of different elastic behaviors such as anisotropy [Bou03], heterogeneity [TW90], non linearity [cB00] and also incompressibility [PB88, Pro97].

An important problem of these models is to choose an appropriate meshing that describes well the object and that does not contain any privileged direction for the strains propagation. Then, the elasticity of springs must be rigorously defined to achieve the desired behavior. Despite this requirement, springs stiffness constants are generally empirically set [NMK*05].

Solutions based on simulated annealing algorithms or genetic algorithms [BSSH03, BSSH04, DKT95, LPC95] give access to spring stiffness constants. Usually they consist in applying random values to different springs constants and in comparing the obtained model with some mechanical experiments in which results are either well known analytically or can be obtained by finite element methods. The stiffness constant of the springs that induce the greatest error is corrected to minimize the discrepancies. However, the efficiency of this process depends on the number of springs and is based on numerous mechanical tests leading to a quite expensive computation time. Moreover, the process should be repeated after any mesh alteration.

Instead of a try-and-error process, a formal solution to parameterize the springs should save computer resources. In this context, two approaches were explored. The Mass-Tensor approach [CDA99, PDA03] aims at simplifying finite element method theory by a discretization of the constitutive equations on each element. Despite its interest, this approach requires pre-computations and the storage of an extensive amount of information for each mesh component (vertex, edge, face, element).

The second approach has been proposed by Van Gelder [Van98] and has been referenced in [Bou03, BO02, Deb00, MBT02, Pal03, Pic01, WV97]. In this approach, Van Gelder proposes a new formulation for triangular meshes, allowing calculating spring stiffness constant according to elastic parameters of the object to simulate (Young's modulus, E, and Poisson's ratio ν). This approach combines the advantages of an accurate mechanical parameterization with a hyper-elastic model, enabling either small or large deformations. However, numerical simulations completed by an Lagrangian analysis exhibited the incompatibility of the proposal with the physical reality. Therefore, it is impossible to use Van Gelder's technique to control realistically the elastic parameters [BBJ*07].

3. Tensile Characteristics and Physical Experiments

Linear elastic isotropic and homogeneous material can be characterized in small deformation by four parameters [Fey64]: the Young's modulus, the Poisson's ratio, the shear modulus and the bulk modulus. These parameters are generally extracted by a set of experiments performed on parallelepiped samples for which geometrical dimensions (x_0, y_0, z_0) at rest are well defined (see Fig.1).
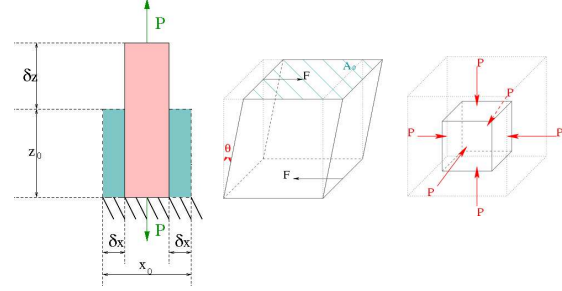

Figure 1: *The three physical experiments: (left) elongation, (middle) shearing and (right) inflation.*

Elongation experiment

The Young's modulus and the Poisson's ratio are measured by elongation experiments. It consists in applying a defined pressure $\vec{P}$ along the z axis of the parallelepiped and measuring the elongations δz along z axis and the thinnings δx and δy along x and y axes (see Fig.1).

The Young's modulus E defines the elasticity of a material by:

$$E = \frac{\left|\vec{P}\right|}{\delta z / z_0}. \tag{1}$$

Young's modulus can vary from 0.39×10^{-3} MPa for lung tissue to $1{,}000{,}000$ MPa for diamond. Poisson's ratio ν characterizes the thinning ($2\delta i / i_0$ with $i \in (x, y)$) induced by the elongation:

$$\nu = - \left(\frac{2\delta i}{i_0}\right) / \left(\frac{\delta z}{z_0}\right). \tag{2}$$

The Poisson's ratio has no unity. It amounts to 0.69 for metals, 0.3 for lungs and 0.5 for incompressible materials.

Shearing experiment

Shear modulus along x axis is measured by applying a force $\vec{F}$ along x to one of the faces orthogonal to z axis, and the opposite force to the other face. The induced deviation angle, noted θ (see Fig.1), characterizes the amplitude of shearing. The shear modulus G is then defined by:

$$G = \left(\frac{\left|\vec{F}\right|}{A_0}\right) / (\tan(\theta)) \sim \left(\frac{\left|\vec{F}\right|}{A_0}\right) / \theta \text{ when } \theta \to 0, \tag{3}$$

with $A_0 = x_0 \times y_0$, the area of the parallelepiped base. Note that, the shear modulus is linked to the Young's modulus and the Poisson's ratio for small deformations by:

$$G = E/2\,(1+\nu). \tag{4}$$

Inflation experiment

Bulk modulus characterizes the response of a material to inflation. Inflation experiments consist in measuring the inflation ΔV resulting from a concentric pressure ΔP, applied to each face of the parallelepiped (see Fig.1).

The bulk modulus B is defined by:

$$B = (\Delta P)\,/\left(\frac{\Delta V}{V_0}\right), \tag{5}$$

where $\Delta V/V_0$ is the volume variation, and ΔP the applied pressure. The bulk modulus is linked to the Young's modulus and the Poisson's ratio for small deformations, with:

$$B = E/3\,(1-2\nu). \tag{6}$$

4. Our 3D Model

The present work aims at reproducing the mechanical behavior of a linear isotropic and homogeneous material with mass-spring systems. We have therefore to determine the stiffness coefficient of the springs so that the mechanical characteristics of the simulated object match the mechanical characteristics of real materials. To set the coefficients, we propose to carry out numerically the experiments described in the previous section, and to establish a relation between the stiffness coefficients and the imposed Poisson's ratio, Young, shear and bulk moduli.

We consider as sample, a parallelepiped with rest dimensions $x_0 \times y_0 \times z_0$. To ensure homogeneous behavior, springs laying on parallel edges need to have the same stiffness constant. Thus, we have to determine only 3 stiffness coefficients for these edges: k_{x_0}, k_{y_0} and k_{z_0}. In addition, some diagonal springs are necessary to reproduce the thinning induced by the sample elongation. Fig.2 displays three possible configurations for these diagonal links:
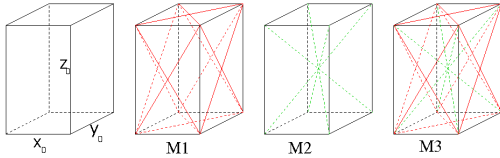

Figure 2: *Three possibilities for the 3D element composition.*

- diagonal springs located on all the faces (configuration M1),
- only the inner diagonals (configuration M2),
- the combination of both inner and face diagonals (configuration M3).

Prior to the above configuration choice, let's present our springs parameterization approach. The determination of the stiffness parameters could be realized by a series of numerical try-and-error processes. This may hardly converge. Therefore, we propose a methodology to calculate these parameters analytically, within the Lagrangian framework, and according to the following procedure.

For each experiment that defines an elastic characteristic (see Fig.1):

1. We build the Lagrangian as the sum of the potential of springs due to elongation as well as the potential of external forces, since kinetic term is null.
2. We establish a Taylor's expansion of the Lagrangian to the second order in deformations and apply the principle of least action. It reads linear equations.
3. We use the definitions of section 3 to express the mechanical characteristics as a function of the stiffness coefficients.
4. We obtain a set of equations, since the mechanical characteristics are input parameters. We solve this system to get stiffness coefficients.

To solve the system, the number of unknowns has to be equal to the number of equations (constraints).

Three equations result from each elongation experiment (one for the Young's modulus and one for the Poisson's ratio along each direction orthogonal to the elongation). Thus, we obtain 9 equations for all the elongation directions. Moreover, 6 more equations have to be added to take into account the shear modulus (6 experiments). We have also to add one more equation to take into account the bulk modulus (1 experiment). Consequently, we could have 16 equations. Since the four elastic characteristics can be linked (see eq. (4) and (6)), if three characteristics are imposed, one can expect that the fourth will be verified. Thus, the whole system admits at most 15 equations.

Three degrees of freedom stem from the parallel edge (k_{x_0}, k_{y_0}, k_{z_0}), but the total number of freedom degrees depends on the diagonal spring configuration. Note that, for small shearing ($\theta \approx 0$), only diagonal springs are stressed. Thus, the Lagrangian equation defining this characteristic depends only on the stiffness constants k_{d_i} of the different diagonals. This means that the diagonal springs constant can be determined independently of the other stiffness coefficients.

Note that, for the configuration (M2), the equations of shearing depend only on the inner diagonal k_d. Consequently, only 3 equations are independent.

We summarize the number of degrees of freedom and the number of equations in Table 1 according to the possible configurations of the system. We observe that all the geometrical configurations bring to an over-constraint system. Nevertheless, the configuration (M2) is less constrained than the others. Thus, we chose this configuration, which corre-

sponds to the model with only the inner diagonals. The four diagonal springs have the same stiffness constant noted k_d.

	M1	M2	M3
Number of unknown stiffness constant in shearing	3	1	4
Number of unknown stiffness constant in elongation	3+(3)	3+(1)	3+(4)
Total number of unknown stiffness constant	6	4	7
Number of equations in elongation	9	9	9
Number of equations in shearing	6	3	6
Total number of equations	15	12	15

Table 1: *Number of equations and unknowns according to the geometry chosen.*

As mentioned above, the inner diagonals fully define the shearing modulus. The problem is that there is only 1 diagonal spring variable for 3 shearing equations (see Table 1). Each equation, corresponding to one particular direction i ($i \in \{x_0, y_0, z_0\}$) leads to a different solution:

$$k_{d_i} = \frac{E\, i \sum_{j \in \{x_0,y_0,z_0\}} j^2}{8(1+\nu)\Pi_{\{l \in \{x_0,y_0,z_0\}, l \neq i\}} l}.$$

However a unique solution can be obtained for a cubic element (*i. e.* with $x_0 = y_0 = z_0$). In this case k_d is well defined proportionally to G:

$$k_d = \frac{3E x_0}{8(1+\nu)}. \tag{7}$$

Thus, we constrain the mesh element to a cube. The non-diagonal edge springs are identical and their spring stiffness constant is noted k_x. This stiffness coefficient has to satisfy two relations (E and ν). One solution can be found for the Poisson's ratio $\nu = 0.25$ but this is not a versatile solution, thus unsatisfying.

Since the number of equations is greater than the number of degrees of freedom, we propose therefore to introduce a new variable. The Poisson's ratio defines the thinning of the sample at a given elongation, *i. e.* it determines the forces orthogonal to the elongation direction. Consequently, by modifying the compression forces, we should achieve, by simulation, the behavior corresponding to any Poisson's ratio ν. We propose to add two new forces induced by the elongation. For the sake of symmetry, the amplitude of the forces is identical in both directions. This amplitude $F_\perp$ is the new degree of freedom (see Fig. 3). Note that this kind of correction is equivalent to the reciprocity principle used in finite elements methods [Fey64].

This new additional variable leads to a system of 2 equations with 2 unknowns. After resolution it reads for $i \in \{x_0, y_0, z_0\}$:

$$k_x = \frac{E x (4\nu + 1)}{8(1+\nu)}, \tag{8}$$

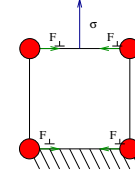$$F_{\perp i} = -\frac{F_i (4\nu - 1)}{16}. \tag{9}$$

Figure 3: *The orthogonal correction force.*

The Lagrangian equation of the inflation test, verifies that this solution satisfies the definition of the bulk modulus.

Since all the stiffness coefficients and the added compressive force are now determined for a mesh element, we can tackle the simulation of any object composed of mesh elements. The simulation of an object results from the simulation of the deformation of each single element that constitutes the object. For this, we need to:

1. Compute all the forces applied to each element. These forces can be (i) internal, including forces due to springs and correction forces, or (ii) external, like gravity or reaction forces due to neighboring elements.
2. Calculate accelerations and velocities according to an integration scheme (explicit or implicit Euler, Verlet, etc.).
3. Displace each mesh node consequently.

Note that, to compute the correction forces applied to a mesh element face, we need to compute the elongation force. This elongation force is the projection on the face normal of the sum of all the external forces applied to the considered face.

Note that, the set of stiffness coefficients and the corrective forces were determined from a Taylor's expansion of the Lagrangian to the second order. This guaranties a correct mechanical behavior for small deformations. The next section will describe numerical experimentations, first to verify that the object has the same mechanical characteristics as each of its composing elements, and second to evaluate the accuracy for deformations attaining 20%.

5. Evaluation of the 3D Model

We propose now to qualify the mechanical properties of our meshed systems for small and large deformations (up to 20%). For this we have carried out several tests. Unless otherwise stated, the object is a parallelepiped composed of cubic mesh elements.

Tensile stress limits

In each tensile experiment, we apply to a beam-like object a quasi-static stress. The elongation can attain 20% of the beam length. The experiments have been carried out with input parameters ranging from 100 Pa to 100 kPa for Young's modulus E, and from 0.1 to 0.5 for Poisson's ratio ν. The accuracy of the simulation is evaluated by comparing the simulated mechanical quantities to the input parameters.

The quantitative study of the test results shows that Young's modulus (see Fig. 4) and Poisson's ratio (see Fig. 5) of our model tend to drift when the deformation increases. Nevertheless, these results are really satisfying. As illustrated in Fig. 4, the error on Young's modulus exceeds 5% only for deformations larger than 10%.
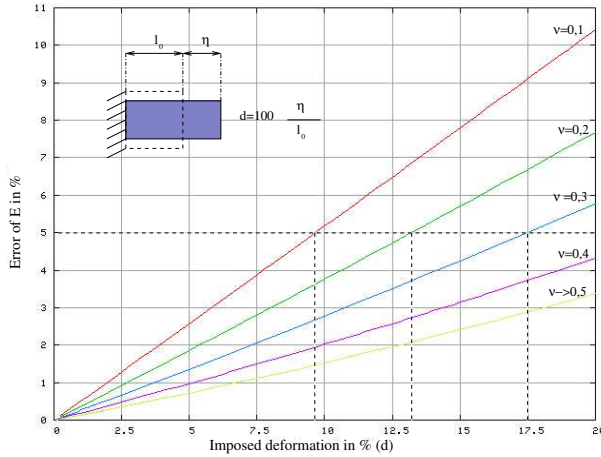

Figure 4: *2D Young's modulus errors for a cubic meshed element in quasi-static tensile stress.*
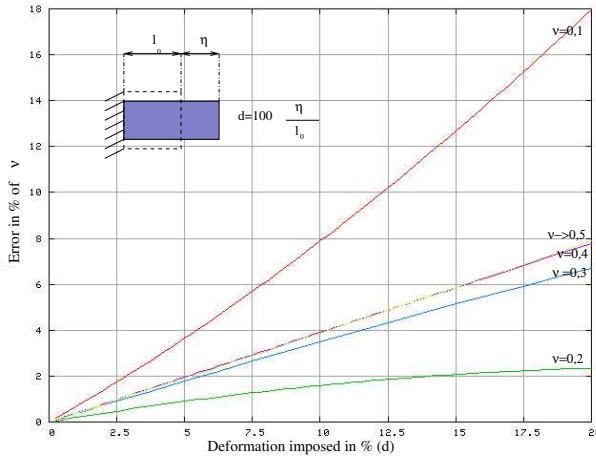

Figure 5: *Poisson's ratio errors (absolute value) for a cubic element in tensile stress.*

Besides, we notice that this error increases conversely with the imposed Poisson's ratio: for a 10% deformation, the error on Young's modulus amounts to 2.7% if $\nu = 0.3$, it amounts only to 2% if $\nu = 0.4$. This error falls down to 1.5% if $\nu = 0.5$.

Concerning Poisson's ratio simulation, the error for $\nu \in [0.3; 0.5]$ remains lower than 5%, even if the deformation attains 14% (see Fig. 5). We observe identical curves whatever

the value of E is. This is not surprising since the spring stiffness constants and the thinning forces are proportional to the input parameter E.

We point out a change in the profile of Poisson's ratio error occurring at $\nu = 0.25$. Thinning is overestimated for the values of $\nu \geq 0.25$ and underestimated elsewhere. In fact, at $\nu = 0.25$ no corrective Lagrangian forces are needed, so the error is minimal.

When performing tensile tests on a beam, meshed by any composition of elements, we obtain exactly the same error as for a unique element. This confirms that the mechanical properties of any meshed object are fully defined by the properties of the mesh elements.

Limits in shearing

Figure 6 presents the results for an element subject to a shearing experience (see Fig. 1). We can remark that the relative error on G does not depend on E, as expected. This error increases with the imposed ν but remains smaller than 5% for a shearing angle inferior to $5°$ and for $\nu < 0.4$. The worst results is obtained for $\nu = 0.5$.
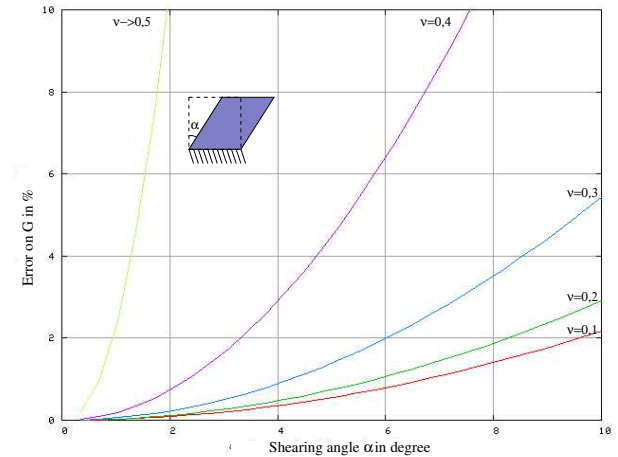

Figure 6: *Measured error on shearing in a cube, according to shearing angle and Poisson's ratio.*

To validate the shearing on an element composition, we built a $100 \times 100 \times 300$ mm beam by assembling elements characterized by $E = 1$ Pa and $\nu = 0.3$. We stressed it by applying a force equivalent to 2000 N. The interpretations of shearing experiment are not straight forward for large deformations. Therefore we considered as reference, a Finite Element Model (FEM) to evaluate the accuracy of our model. For this, the results of our simulations and the FEM reference have been superimposed (see Fig. 7). Within the theoretical framework of our model, *i. e.* small deformations, the agreement is very satisfactory, attesting the good behavior of our model.
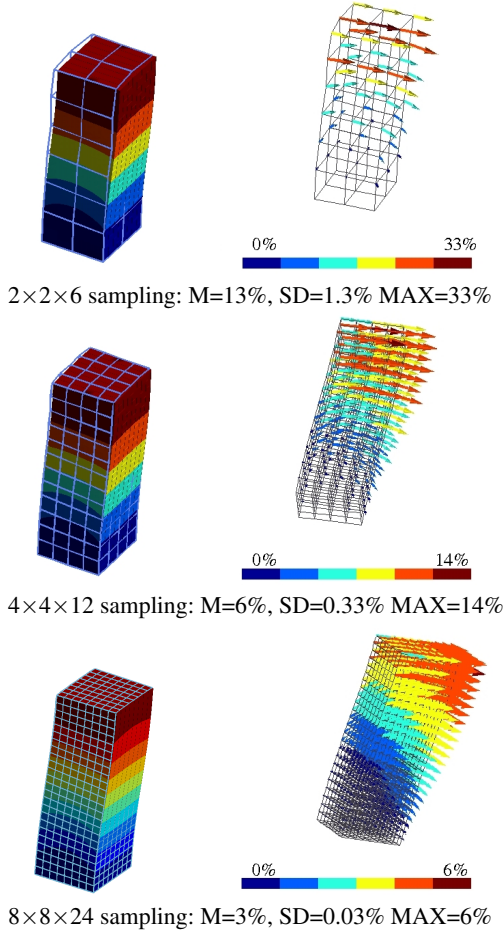
2×2×6 sampling: M=13%, SD=1.3% MAX=33%

4×4×12 sampling: M=6%, SD=0.33% MAX=14%

8×8×24 sampling: M=3%, SD=0.03% MAX=6%

Figure 7: *Shearing experience: (Left) superimposition of the results of our wired model with the color gradation FEM reference solution and (Right) Map of error in displacement on each node of the mesh. Notation: M for mean error value, SD for standard deviation and MAX for maximal error.*

To get a more quantitative comparison, we quantified at each node of the mesh the discrepancy between the displacements calculated by our model and the displacements extracted from the finite element reference. We obtained a map of errors in which the mesh illustrate the solution of our model, and the arrows represent the enhanced discrepancies with regard to finite element reference.

Fig. 7 illustrates the influence of the mesh resolution on the result accuracy. We observe the mean error amounts to about 13% with a maximum of 33% for a 2×2×6 resolution. It decreases progressively, if we improve the resolution. Mean error and the maximal error fall down respectively to 3% and 6% for a 8×8×24 resolution.

Limits in inflation

We also performed some tests of deflation and inflation to measure the error in the bulk modulus conservation (see

Fig. 8). These experiments exhibit a conservation of this coefficient for small displacements whatever the imposed coefficient E and ν are. Conservation is observed whatever the composition of elements is.
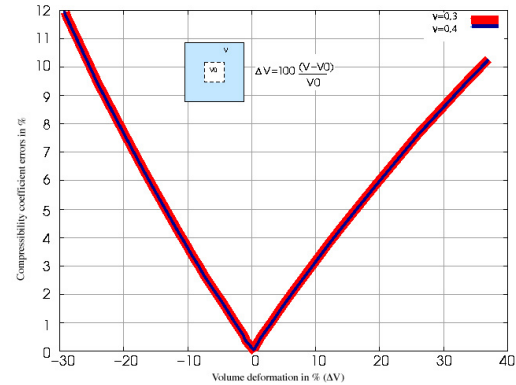

Figure 8: *Error measured on the bulk modulus according to the deformation imposed in volume.*

Limits in deflection

The deflection experience (construction or structural element bends under a load) is recommended to validate mechanical models. It constitutes a relevant test to evaluate (a) the mass repartition, and (b) the behavior in case of large deformations (inducing large rotations, especially close to the fixation area).

This test consists in observing the deformation of a beam anchored at one end to a support. At equilibrium, under gravity loads, the top of the beam is under tension while the bottom is under compression, leaving the middle line of the beam relatively stress-free. The length of the zero stress line remains unchanged (see Fig. 9).
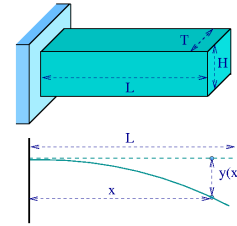

Figure 9: *Cantilever submitted to gravity, expression of the neutral axis deviation.*

In case of a null Poisson's ratio, the load induced deviation of the neutral axis is given by:

$$y(x) = \frac{\rho g}{24\,EI} \left(6\,L^2 x^2 - 4\,L\,x^3 + x^4 \right) \qquad (10)$$

for a parallelepiped beam of inertia moment $I = TH^3/12$, and with linear density $\rho = M/L$.

We notice that results are dependent of the sampling resolution, as for any other numerical method, however the fiber axis profile keeps close to the profile given by the equation (10). Figure 10 displays some results for a cantilever beam of dimensions $400 \times 100 \times 100$ mm, with Young's modulus equals to 1000 Pa, Poisson's ratio to 0.3 and a mass of 0.0125 Kg.m^{-3}. By looking at the displacement errors at each mesh node, we observe that the error is decreasing when the sampling is improved: the maximum error in the sampling $4 \times 1 \times 1$ is about 45% while it is about 5% for a resolution of $16 \times 4 \times 4$.
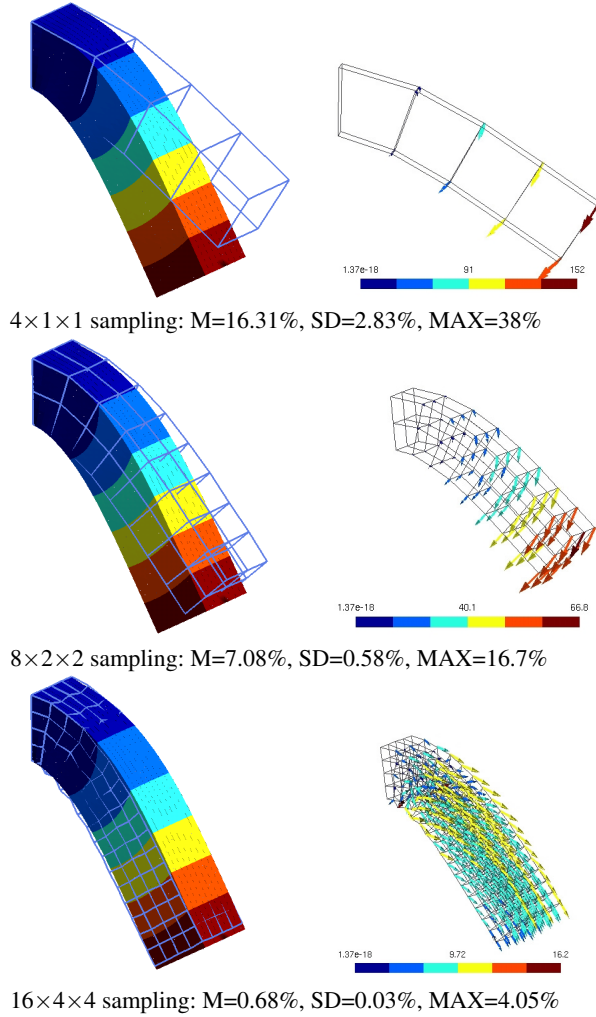

$4 \times 1 \times 1$ sampling: M=16.31%, SD=2.83%, MAX=38%

$8 \times 2 \times 2$ sampling: M=7.08%, SD=0.58%, MAX=16.7%

$16 \times 4 \times 4$ sampling: M=0.68%, SD=0.03%, MAX=4.05%

Figure 10: *Deflection experiment: (Left) the reference FEM solution (in color gradation) with superimposition of various simulations performed for different sampling resolutions (wire mesh), (Right) Map of error in displacement on each node of the mesh with the scale indicating the minimal error (in blue) and maximal (in red). Notation: M for mean error values, SD for standard deviation and MAX for maximum error.*

Nevertheless figure 11 illustrates that there is a limit to the sampling resolution beyond which large shearings (rotations) of meshes in the vicinity of the fixation area are observed. In this area, our model is outside of its domain of validity and the maximum of error is about 8%. However, our model behaves better than the models using finite element methods that prove more difficulty outside their validity domain.
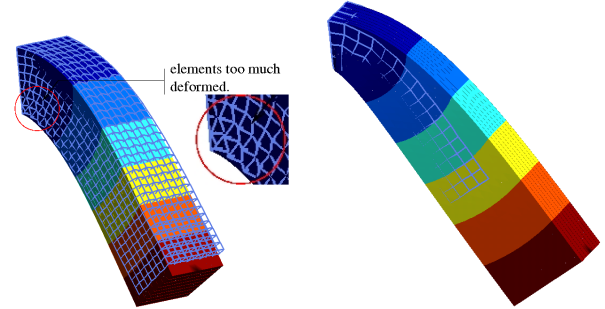

Figure 11: *(Left) Limit of the sampling resolution: the quality of results is limited by the deformations accepted by our model. (Right). Results of the cantilever experiment are totally wrong for small deformation conditions with finite element. However, our model results (in wire frame) remain within an acceptable range.*

Illustration on a non-symmetric composition

All the previous tests were performed on highly symmetric objects. We propose now to break this symmetry. Figure 12 presents L-like object fixed at its base.
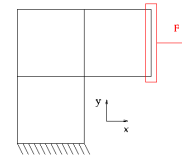

Figure 12: *Experiment on a non-symmetric object.*

We apply a constant force to the edges that are orthogonal to the base. Figure 13 shows our results superimposed to the FEM solution, with a map of error in displacement. The object dimensions are $4000 \times 4000 \times 4000$mm. The mechanical characteristics are: Young's modulus = 1kPa, Poisson's ratio = 0.3 and an applied force = 0.3GN. In this experiment, we have neglected the mass. Again we clearly observe that our model behaves as expected: better mesh resolution leads to better results. Moreover, the dissymmetry of the geometry does not influence the accuracy of the results.
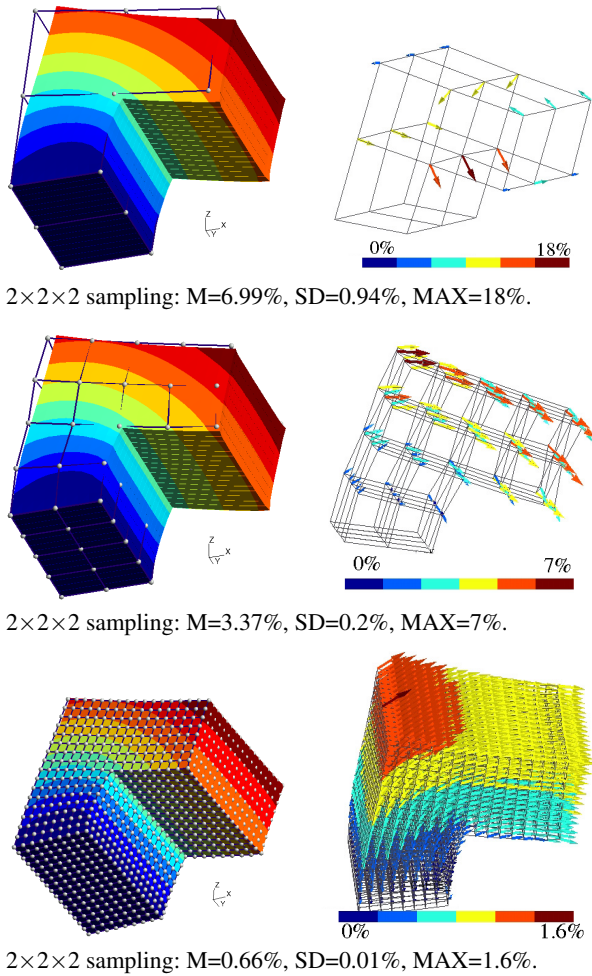
2×2×2 sampling: M=6.99%, SD=0.94%, MAX=18%.

2×2×2 sampling: M=3.37%, SD=0.2%, MAX=7%.

2×2×2 sampling: M=0.66%, SD=0.01%, MAX=1.6%.

Figure 13: *Experiment on a non-symmetric object: (Left) the reference FEM solution (in color gradation) with superimposition of various simulations performed for different mesh resolutions), (Right) map of error in displacement (in mm) on each node of the mesh. Notation: M for mean error value, SD for standard deviation, MAX for maximum error.*

6. Conclusion and Future Work

We proposed a mass-spring model that ensures fast and physically accurate simulation of linear elastic, isotropic and homogeneous material. It consists in meshing any object by as set of cubic mass-spring elements, and in adding some corrective forces orthogonal to elongation forces. By construction, our model is well characterized by the Young's modulus, Poisson's ratio, shearing modulus and bulk modulus, for small deformations. The spring coefficients have just to be initialized according to simple analytic expressions. The amplitude of the corrective forces is simply derived from the elongation forces. Limits of our model have

been given, by comparing our results with those obtained by a finite element method, chosen as reference for preciseness.

We exhibited that our model can also support large deformations. The accuracy increases with the mesh resolution.

In the future, we are looking to apply the same technique to other geometrical elements, for example parallelepipeds, tetrahedron or any polyhedron. This would increase the geometrical reconstruction possibilities and would offer more tools for simulating complex shapes.

Mesh optimization or local mesh adaptation would probably improve the efficiency of the model. For example, we can modify the resolution in the vicinity of highly deformed zones, reducing large rotations of elements undergoing heavy load.

Moreover, it may be interesting to investigate a procedure to update the spring coefficients and corrective forces when the deformations become too large.

References

[AT00] AUBEL A., THALMANN D.: Realistic deformation of human body shapes. In *Computer Animation and Simulation '00* (2000), pp. 125–135.

[BBJ*07] BAUDET V., BEUVE M., JAILLET F., SHARIAT B., ZARA F.: *A New Mass-Spring System Integrating Elasticity Parameters in 2D*. Tech. Rep. RR-LIRIS-2007-003, LIRIS UMR 5205 CNRS/INSA de Lyon/Université Claude Bernard Lyon 1/Université Lumière Lyon 2/Ecole Centrale de Lyon, Villeurbanne, France, February 2007. http://liris.cnrs.fr/publis/?id=2683.

[BO02] BRUYNS C., OTTENSMEYER M.: Measurements of soft-tissue mechanical properties to support development of a physically based virtual anima model. In *MICCAI 2002* (2002), pp. 282–289.

[Bou03] BOURGUIGNON D.: *Interactive Animation and Modeling by Drawing - Pedagogical Applications in Medicine*. PhD thesis, Institut National Polytechnique de Grenoble, 2003.

[BSSH03] BIANCHI G., SOLENTHALER B., SZÉKELY G., HARDERS M.: Mesh topology for mass-spring models. In *MICCAI 2003* (Berlin, 2003), Springer-Verlag, (Ed.), pp. 50–58.

[BSSH04] BIANCHI G., SOLENTHALER B., SZÉKELY G., HARDERS M.: Simultaneous topology and stiffness identification for mass-spring models based on FEM reference deformations. In *MICCAI 2004* (Berlin, 2004), Springer-Verlag, (Ed.), pp. 293–301.

[cB00] COIS BOUX DE CASSON F.: *Simulation dynamique de corps biologiques et changements de topologie interactifs*. PhD thesis, Université de Savoie, 2000.

[CDA99] COTIN S., DELINGETTE H., AYACHE N.: Efficient linear elastic models of soft tissues for real-time

surgery simulation. *Proceedings of the Medecine Meets Virtual Reality (MMVR 7) 62* (1999), 100–101.

[CHP89] CHADWICK J., HAUMANN D., PARENT R.: Layered construction for deformation animated characters. *Computer Graphics 23*, 3 (1989), 243,252.

[Deb00] DEBUNNE G.: *Animation multirésolution d'objets déformables en temps réel, Application à la simulation chirurgicale.* PhD thesis, Institut National Polytechnique de Grenoble, 2000.

[DKT95] DEUSSEN O., KOBBELT L., TUCKE P.: Using simulated annealing to obtain good nodal approximations of deformable objects. In *Proceedings of the Sixth Eurographics Workshop on Animation and Simulation* (Berlin, 1995), Springer-Verlag, (Ed.), pp. 30–43.

[Fey64] FEYNMAN R.: *The Feynman Lectures on Physics*, vol. 2. Addison Wesley, 1964. chapter 38.

[KEH04] KECKEISEN M., ETZMUQ., HAUTH M.: Physical models and numerical solvers for cloth animations. In *Simulation of Clothes for Real-time Applications* (2004), vol. Tutorial 1, INRIA and the Eurographics Association, pp. 17–34.

[LJF*91] LUCIANI A., JIMENEZ S., FLORENS J. L., CADOZ C., RAOULT O.: Computational physics: A modeler-simulator for animated physical objects. In *Proceedings of Eurographics 91* (Amsterdam, 1991), Eurographics, pp. 425,436.

[LPC95] LOUCHET J., PROVOT X., CROCHEMORE D.: Evolutionary identification of cloth animation models. In *Proceedings of the Sixth Eurographics Workshop on Animation and Simulation* (Berlin, 1995), Springer-Verlag, (Ed.), pp. 44–54.

[MBT02] MACIEL A., BOULIC R., THALMANN D.: Deformable tissue parameterized by properties of real biological tissue. citeseer.nj.nec.com/574309.html, 2002.

[MC97] MESEURE P., CHAILLOU C.: Deformable body simulation with adaptative subdivision and cuttings. In *5th Int. Conf. in Central Europe on Comp. Graphics and Visualisation WSCG'97* (1997), pp. 361–370.

[Mil88] MILLER G.: The motion dynamics of snakes and worms. *Computer Graphics 22*, 4 (1988), 168,178.

[MLM*05] MEIER U., LÓPEZ O., MONSERRAT C., JUAN M. C., ALCAÑIZ M.: Real-time deformable models for surgery simulation : a survey. *Computer Methods and Programs in Biomedicine 77*, 3 (2005), 183–197.

[NMK*05] NEALEN A., MˊULLER M., KEISER R., BOXERMAN E., CARLSON M.: Physically based deformable model in computer graphics. *Eurographics* (2005). State of the Art report.

[NT98] NEDEL L. P., THALMANN D.: Real-time muscles deformations using mass-spring systems. *Computer Graphics International* (1998), 156–165.

[Pal03] PALOC C.: *Adaptative Deformable Model (allowing Topological Modifications) for Surgical Simulation.* PhD thesis, University of London, 2003.

[PB88] PLATT J., BARR A.: Constraint methods for flexible models. *Computer Graphics 22*, 4 (1988), 279–288.

[PBP96] PROMAYON E., BACONNIER P., PUECH C.: Physically based deformation constrained in displacements and volume. In *Proceedings of Eurographics'96* (Oxford, 1996), BlackWell Publishers.

[PDA03] PICINBONO G., DELINGETTE H., AYACHE N.: Non-linear anisotropic elasticity for real-time surgery simulation. *Graphical Model* (2003).

[Pic01] PICINBONO G.: *Modèles géométriques et physiques pour la simulation d'interventions chirurgicales.* PhD thesis, Université de Nice Sophia-Antipolis, Feb. 2001. http://www.inria.fr/rrrt/tu-0669.html.

[Pro95] PROVOT X.: Deformation constraints in a mass-spring model to describe rigid cloth behavior. In *Proceedings of Graphics Interface 95* (Toronto, 1995), Canadian Human-Computer Communications Society, pp. 147,154.

[Pro97] PROMAYON E.: *Modélisation et simulation de la respiration.* PhD thesis, Université Joseph Fourier, Grenoble, 1997.

[TW90] TERZOPOULOS D., WATERS K.: Physically-based facial modelling, analysis, and animation. *The Journal of Visualization and Computer Animation 1* (1990), 73–80.

[Van98] VAN GELDER A.: Approximate simulation of elastic membranes by triangulated spring meshes. *Journal of Graphics Tools 3*, 2 (1998), 21–42.

[WV97] WILHELMS J., VAN GELDER A.: Anatomically based modelling. In *Computer Graphics (SIGGRAPH'97 Proceedings)* (1997), pp. 173–180.